Frequency-Agile and Spectrally Sensitive Radar Transmitter Amplifier Optimizations

Charles Baylis, Robert J. Marks II, Lucilia Hays, Zachary Hays, Sarvin Rezayat, Christopher Kappelmann
Department of Electrical and Computer Engineering
Baylor University
Waco, Texas, USA
Charles_Baylis@baylor.edu

Mohammad Abu Khater, Abbas Semnani, Dimitrios Peroulis
Department of Electrical and Computer Engineering
Purdue University
West Lafayette, Indiana, USA
dperouli@purdue.edu

Edward Viveiros
U.S. Army Research Laboratory
Adelphi, Maryland, USA
edward.a.viveiros2.civ@mail.mil

***Abstract*—The design and implementation of a first generation evanescent-mode cavity impedance tuner for reconfigurable radar transmitters is presented. The impedance tuner is capable of handling 90 W of radio-frequency (RF) power. The tuner can be used as a reconfigurable load matching network for an amplifier device to maximize the power-added efficiency (PAE) while meeting adjacent-channel power ratio (ACPR) or spectral mask constraints. Algorithms expected to be useful in fast tuning of this device are described, including a modified gradient approach for the optimization of the PAE while meeting constraints on the ACPR. Instead of tuning based on the reflection coefficient, which requires pre-characterization of the tuner, the resonant cavity position numbers of the tuner can be directly adjusted. Initial results are shown using an interval-halving search for optimization of PAE that directly tunes the cavity position numbers to optimize the tuner. This search is more resilient to drift and other repeatability issues that influence characterization. The fast optimization of this tuner is designed to give radar transmitter power amplifiers frequency agility in congested spectral environments.**

Keywords—Evanescent-mode cavity resonator, power amplifier, optimization, impedance tuner, reconfigurable circuit, radar systems, spectrum

I. Introduction

Future radar systems must be adaptive and reconfigurable to meet the demands of the dynamic wireless spectrum. Spectrum allocation is moving toward a dynamic spectrum access model, where spectrum is allocated in real time based on needs of members of a system of systems. Adaptive radar [1]-[2] and cognitive radar [3]-[4] systems are capable of responding dynamically to the surrounding environment. To implement an adaptive and reconfigurable radar transmitter, the RF circuitry of the radar transmitter must be reconfigurable [5]. Because of the large amount of power required by the transmitter's power amplifier, its efficiency is of significant importance, and its performance can be maximized by tuning it in real-time with a tunable matching network [5]-[6].

While reconfigurable amplifiers have been widely demonstrated for use in communication systems, their use for radar transmitters has been viewed with skepticism due to the high power-handling requirements of radar applications. However, recent developments in tunable circuits show the potential for higher power handling [7]-[8]. We recently demonstrated an evanescent-mode (EVA) cavity tuner capable of handling 90 W of RF power [9]. This demonstrates significant advancement of the state-of-the-art toward power levels necessary for radar applications. Plasma devices may be used in the future to further increase output power capabilities [10].

II. Next-Generation Radar Transmitter

The work described herein has been performed to develop capabilities for reconfigurable amplifiers in the framework of a next-generation radar transmitter concept illustrated in Fig. 1 [11]. A reconfigurable amplifier with a tunable load matching network will be needed in order to optimize the amplifier performance for dynamically varying operating frequency assignments, changing bandwidths, and different waveforms resulting from changing range/Doppler resolution objectives. The tunable amplifier and matching network will be controlled by an Field Programmable Gate Array (FPGA), along with a signal generator that can vary the amplifier input waveform. The amplifier output should be measured by an on-device power sensor to assess output power and efficiency and a spectrum analyzer to verify compliance with spectral requirements.

The reconfigurable power amplifier must be able to withstand large amounts of RF power, and must also be able to quickly adjust the impedance presented to the amplifier device. The amplifier is a key building block for spectrum compatibility. To produce the large power levels needed for radar applications with high power efficiency, the amplifier must typically be operated in its nonlinear region, causing significant spectral spreading due to intermodulation. In range radar applications where a high bandwidth is desirable for good

range resolution, this presents challenges in meeting spectral mask requirements.

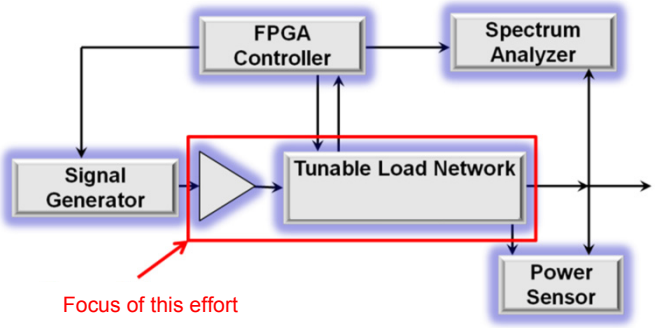

Fig. 1. Adaptive and reconfigurable radar transmitter [11]. The reconfigurable amplifier with a tunable load matching network is the focus of the work described herein..

The adaptive and reconfigurable radar amplifier should ultimately be capable of simultaneously optimizing its circuitry and output waveform to achieve (1) desirable range/Doppler resolution characteristics, (2) high PAE, and (3) a spectrally compliant output waveform.

III. High-Power Tuner Technology

A high-power reconfigurable impedance tuner was designed using tunable EVA cavity resonator technology implemented in a substrate integrated waveguide (SIW). Figure 2 shows the layout of the tuner, composed of two coupled and independently controlled resonant cavities. In each resonator, a piezo actuator can move up and down to adjust the resonant frequency of the tuner by changing the gap size over a capacitive post in the center of the resonator. The piezo discs are placed atop silver epoxy layers, which sit on top of copper foils. Figure 3 shows a multilevel layout of the impedance tuner with dimensions. The height of each cavity is 1.27 mm, with cavity radius of 6.6 mm and post height of 1.5 mm. The total board thickness is 1.34 mm [9].

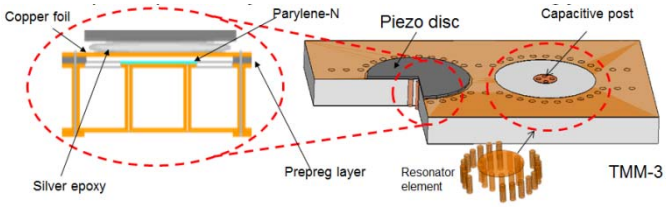

Fig. 2. Substrate integrated waveguide cavity resonator tuner layout

Monitoring and control functions are performed using a monitoring resonator placed atop the tuning resonator. As the disc is raised, increasing the gap of the primary resonant cavity, the gap of the monitoring resonator is decreased, lowering its resonant frequency. As such, the decrease in resonant frequency of the monitoring resonator can be used to determine the increase in resonant frequency of the primary resonator. Figure 4 shows that the monitoring resonator is the reference for an oscillator. The oscillator's output is frequency divided todiscern the frequency of oscillation and this information is provided to a control system [8].

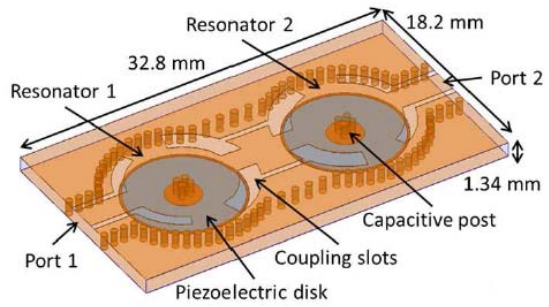

Fig. 3. Tuner multilevel layout , including capacitive posts, with dimensions, reprinted from [9].

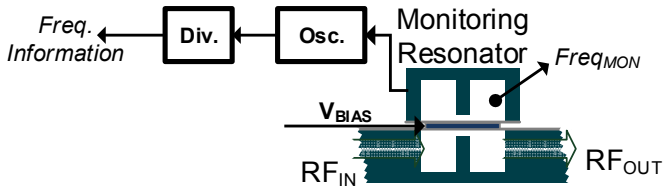

Fig. 4. Discernment of the resonant frequency using a monitoring resonator, oscillator, and frequency divider (similar to [8]).

The two-pole impedance tuner, implemented using the SIW structure, is shown in Fig. 5, where coaxial connectors are employed for external connections. Figure 6 shows the completed tuner system, including the tuner with monitoring resonators, the oscillator and frequency divider, a charge pump, a FPGAcontroller, and a Universal Serial Bus (USB) interface. This tuner was packaged for simple portability, as shown in Fig. 7.

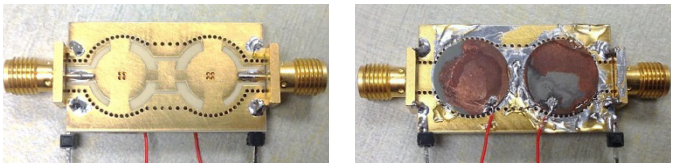

(a) (b)

Fig. 5. Resonant impedance tuner circuit, including (a) bottom view and (b) top view including the attached piezo discs. Reprinted from [9].

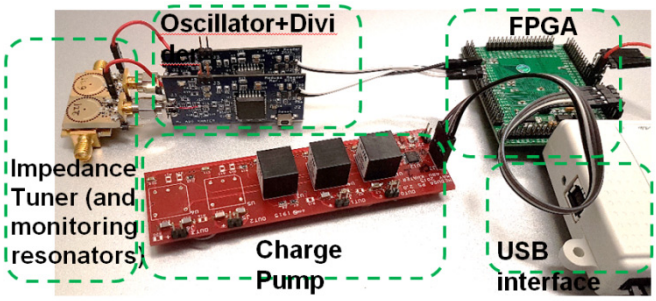

Fig. 6. Complete impedance tuner system, including the tunable circuit with monitoring resonators, the oscillator and frequency divider, anFPGAcontroller, and a USB interface. Reprinted from [9].

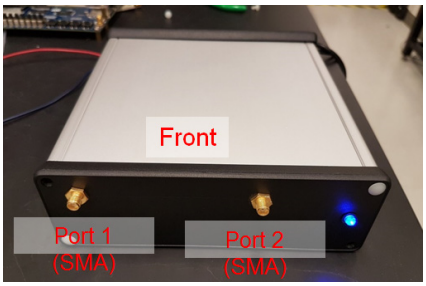

Fig. 7. Packaged impedance tuner system with SMA input and output connectors

A tuner characterization was performed to assess the coverage of the Smith Chart. Simulated and measured values of the tuner input reflection coefficient at 3.3 GHz are shown in Figures 8(a) and 8(b), respectively. The tuner demonstrates excellent coverage of the Smith Chart, with the exception of a small circle in the upper right corner. This "circle of unreachable reflection coefficient states" can be rotated to any desired location, where it will then be away from the region of interest, by placing a variable phase shifter between the amplifier device and the tuner in the final system.

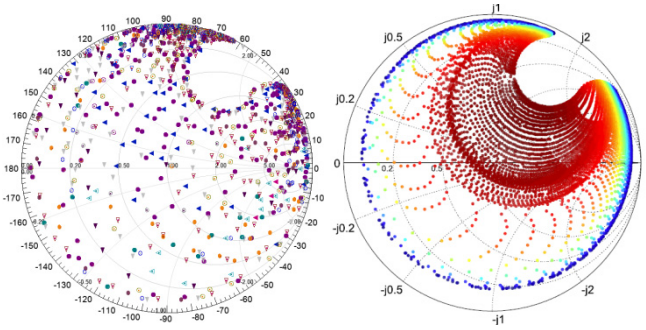

(a) (b)

Fig. 8. (a) Simulated (reprinted from [9]) and (b) measured tuner input reflection coefficient values at 3.3 GHz

Figure 9 demonstrates the power handling capability of the device. Figure 9(a) shows that the tuner loss is nearly constant until 40 dBm (10 W) of input power and then starts to increase. This increase is actually related to the compression of the employed power amplifier for this measurement. No gas breakdown, which is the main concern of high-power capability, was observed, which indicates that the device can provide reliable performance up to at least 90 W. Figure 9(b) shows the tuner transmission coefficient over the frequency range from 2 GHz to 4.5 GHz at different values of input power. This measurement shows that the tuner possesses good transmission in a 50 Ω environment (using large $|S_{21}|$ as the metric) from near 2.9 GHz to 3.3 GHz with input power up to about 90 W.

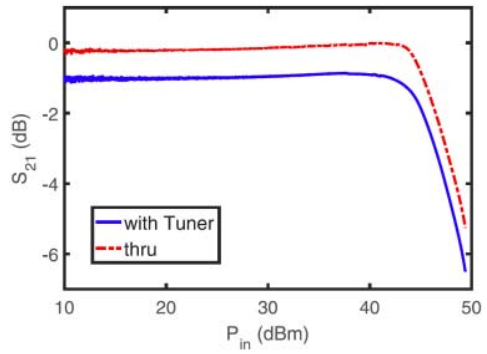

(a)

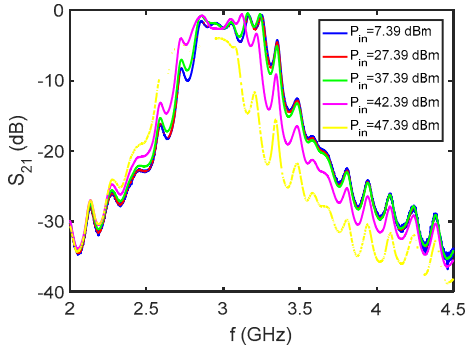

(b)

Fig. 9. (a) Transmission coefficient magnitude (a) versus input power and (b) over frequency for different input power values.

IV. Fast Optimization Algorithms for Tuner Use

The tuner can be optimized using a direct constrained optimization search algorithm, as described initially by Fellows [12] and applied to the high-power tuners by Hays [13]. The algorithms are based on estimating the gradients of the PAE and ACPR, as shown in Fig. 10. The gradients are estimated by measuring Γ_L just to the right and just above the candidate Γ_L in the Smith chart. From the gradient estimations of ∇p (PAE gradient) and ∇a (ACPR gradient), the optimum travel directions for PAE and ACPR are given as follows, respectively [12]:

$$\hat{p} = \frac{\nabla p}{|\nabla p|}, \tag{1}$$

$$\hat{a} = -\frac{\nabla a}{|\nabla a|}. \tag{2}$$

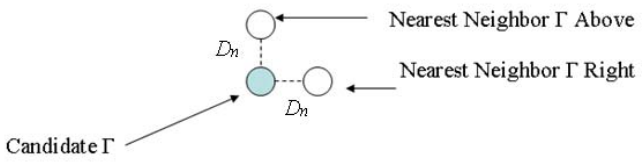

Fig. 10. Neighboring-point measurements for estimation of the PAE and ACPR gradients in the Smith chart

Equation (2) contains a negative sign, because the optimum ACPR direction is in the direction of ACPR steepest ascent,

whereas the optimum PAE direction is in the direction of PAE steepest ascent and does not require a negative sign.

The goal of the optimization is to find the value of Γ_L that obtains the maximum PAE while providing an ACPR less than a pre-specified constraint value, $ACPR_{limit}$. The construction of the search vector $\bar{v}$ to the next candidate is based on the $\hat{p}$ and $\hat{a}$ vectors as follows [12]:

$$\bar{v} = \hat{a}D_a + \hat{b}D_b, \tag{3}$$

for cases where $ACPR > ACPR_{limit}$ (out of compliance) and

$$\bar{v} = \hat{p}D_a + \hat{b}D_b, \tag{4}$$

for cases where $ACPR \leq ACPR_{limit}$ (in compliance). The magnitudes of the vector components are defined as follows [12]:

$$D_a = \frac{D_s}{2}\frac{|ACPR_{cand} - ACPR_{limit}|}{|ACPR_{worst} - ACPR_{limit}|}, \tag{5}$$

$$D_b = \frac{D_s}{2}\frac{|\theta_{cand} - 90°|}{90°}, \tag{6}$$

Figure 11 shows the search vector construction in the two scenarios.

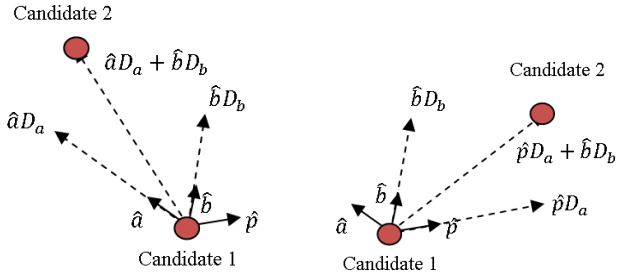

Fig. 11. Search vector construction for (a) ACPR out of compliance and (b) ACPR in compliance. Reprinted from [12] for convenience.

Prior to demonstration on the high-power tuner, the search algorithm was successfully demonstrated using a traditional load-pull measurement test bench with mechanical tuners from Maury Microwave. A Skyworks packaged amplifier was used as the device under test. Figures 12 and 13 show fast search algorithm measurement results starting from two different starting Γ_L values [12]. The fast measurement search starting from $\Gamma_L = 0$ converges in only 13 measurements (Fig. 12(a)), while the fast measurement search starting from Γ_L =0.9/180° converges in only 22 measurements. Both results attain similar PAE values (6.881% and 6.529%, respectively) [12].

In using this algorithm on the high-power tuner, several issues come to bear. These include the repeatability and stability of the tuner, as well as the characterization density. However, the Γ_L based search algorithm is still effectively used through the use of some strategic techniques, described in a recently submitted journal manuscript [13].

Device input power [14] and bias voltage [15] can be co-optimized with load impedance to obtain even better efficiency results and spectral performance. The Smith Tube allows the plotting of an additional component as a vertical axis in addition to the standard Smith Chart, which is shown in the horizontal plane. Figure 13 shows the Power Smith Tube and the Bias Smith Tube.

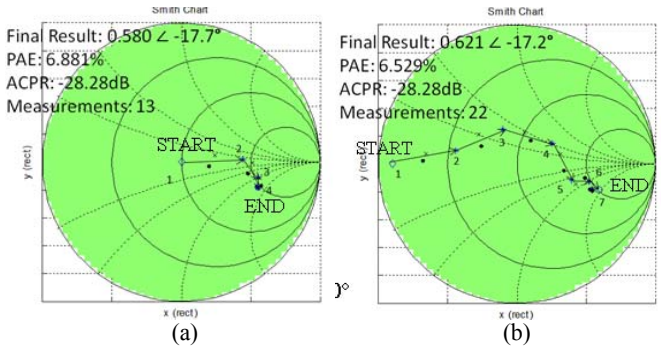

Fig. 12. Skyworks packaged amplifier fast search algorithm measurement results from starting points (a) $\Gamma_L = 0$, (b) Γ_L = 0.9/180°. Reprinted from [12].

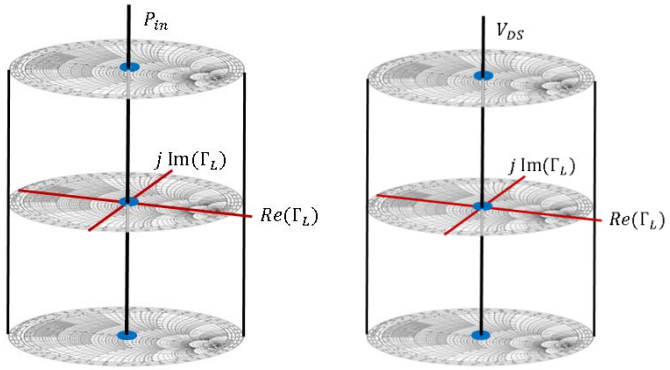

Fig. 13. (a) Power Smith Tube [14] and (b) Bias Smith Tube [15]

The PAE and ACPR are significantly dependent on Γ_L, input power P_{in}, and, for a field-effect transistor (FET), both the drain-source bias voltage V_{DS} and the gate-source bias voltage V_{GS}. As such, the quickest way to find an optimum solution is to tune the parameters simultaneously.

Figure 14 shows results from a simultaneous optimization of Γ_L and P_{in} in the Power Smith Tube for a Microwave Technologies MWT-173 FET. The search was performed to maximize PAE while maintaining ACPR ≤ -40 dBc [14].

In tuning the resonant cavities, another approach is to directly tune the resonant cavity position numbers, as described in a recent conference paper [16]. This removes the issue of the characterization's repeatability, which is based on the tuner's sensitivity to movement and temperature changes. A first-step experiment was performed by optimizing only for PAE, with no ACPR constraint. An interval-halving approach to optimizing the resonant cavity position numbers for maximum PAE is shown in Fig. 15. The interval halving is performed first on the position number for cavity 1 (n_1), followed by the position number for cavity 2 (n_2). For each position number, n, the minimum value n_{min} and maximum value n_{max} are specified. A measurement is then performed at the center position number of the interval (n_c). A value is then measured at a slightly greater value $n_c + n_n$. If the PAE value is greater at $n_c + n_n$, then the interval is halved upward,

selecting n_{next} as the next point for measurement halfway between n_c and n_{max}, as shown in Fig. 15(a). If instead the PAE value is lower at $n_c + n_n$ than at n_c, then the interval is halved downward, with n_{next} selected as the next point for measurement halfway between n_{min} and n_c, as shown in Fig. 15(b). The interval halving process continues successively until the PAE changes less than 1 percent in moving from the center point of one interval to the center point of the next (smaller) interval during the halving process [16].

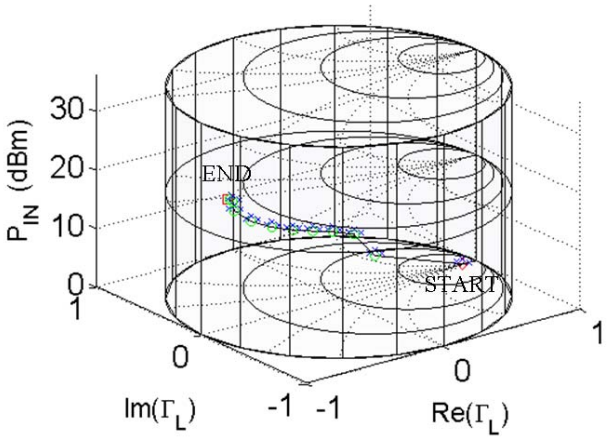

Fig. 14. Fast joint optimization of Γ_L and P_{in} using the Power Smith Tube from starting point Γ_L = 0.9/0°, P_{in} = 0 dBm. The search endpoint is Γ_L = 0.77 / 176.4° and P_{in} = 21.21 dBm, giving PAE = 41.44% and ACPR = -40.05 dBc. Reprinted from [14].

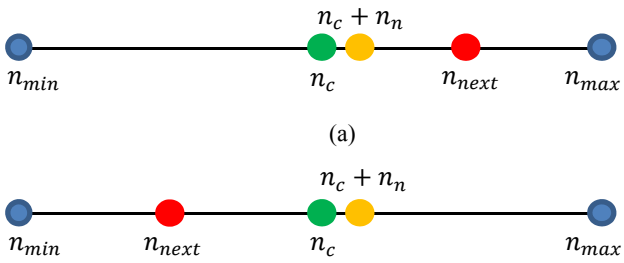

Fig. 15. Tuner search algorithm using interval halving of each resonant cavity position number n. Interval halving is performed successively for n_1, the position number of resonant cavity 1, and n_2, the position number of resonant cavity 2. Reprinted from [16].

Figure 16 shows the results of an interval halving search performed for an MWT-173 FET with bias V_{GS} = -1.5 V, V_{DS} = 4.5 V, and P_{in} = 14 dBm. The search converged to a PAE of 20.78% at n_1 = 7147, n_2 = 7902, with a total of 22 measurements in the search. The Smith Chart trajectory for the search (plotting the values of Γ_L corresponding to the combinations (n_1, n_2) used in the search) is shown in Fig. 17.

Ongoing research involves the development of a constrained vector-based modified gradient algorithm that will effectively work in the resonant cavity position-number plane. Some challenges have resulted from trying to incorporate the modified gradient search algorithm used previously in the Smith Chart to the (n_1, n_2) plane, due to contour nonconvexities often observed in the (n_1, n_2) plane. An approach to optimize Γ_L using a characterization of the high-power tuner is also discussed in a recent paper submission [17].

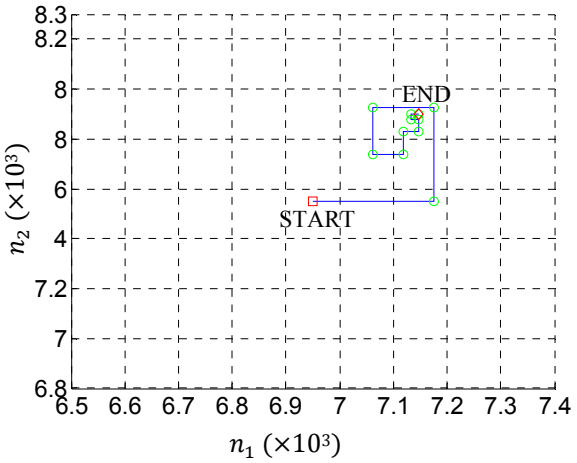

Fig. 16. Resonant cavity position number interval-halving search measurement results for an MWT-173 FET at f = 3.3 GHz, V_{GS} = -1.5 V, V_{DS} = 4.5 V, and P_{in} = 14 dBm. A maximum PAE of 20.78% was found for n_1 = 7147, n_2 = 7902 (estimated Γ_L = 0.10/148.5°), with 22 total measurements. Reprinted from [16].

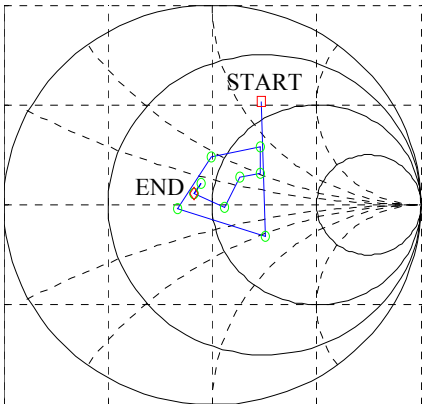

Fig. 17. Smith chart search trajectory for the Fig. 16 search. Reprinted from [16].

V. Conclusions

A reconfigurable EVA cavity tuner capable of handling 90 W of RF power has been demonstrated, along with optimization algorithms that will be useful to provide real-time reconfigurability. The tuner has been designed as a first step toward constructing an adaptive, reconfigurable radar transmitter. An interval-halving search using direct tuning of the resonant cavity position numbers is demonstrated to maximize the PAE of the amplifier device. In addition, a vector-based, modified gradient search previously demonstrated using traditional load-pull tuners is expected to be used in maximizing the PAE while meeting the constraints of the ACPR . Fast optimization techniques will allow the tuner to adjust its behavior in response to dynamically changing spectral requirements in a congested spectral environment.

ACKNOWLEDGMENTS

This work has been funded by the Army Research Laboratory (Grant No. W911NF-16-2-0054) and the National Science Foundation (Grant No. ECCS-1343316). The views and opinions expressed do not necessarily represent the opinions of the U.S. Government. The authors are grateful to John Clark of the Army Research Laboratory for assistance in development of this paper.

REFERENCES

[1] L.E. Brennan and I.S. Reed, "Theory of Adaptive Radar," *IEEE Transactions on Aerospace and Electronic Systems*, Vol. 9, No. 2, March 1973, pp. 237-252.

[2] J.S. Goldstein and I.S. Reed, "Theory of Partially Adaptive Radar," *IEEE Transactions on Aerospace and Electronic Systems*, Vol. 33, No. 4, October 1997, pp. 1309-1325.

[3] S. Haykin, "Cognitive Radar: A Way of the Future," *IEEE Signal Processing Magazine*, January 2006, pp. 30-40.

[4] J. Guerci, *Cognitive Radar: The Knowledge-Aided Fully Adaptive Approach*, Artech House, 2010.

[5] N. Kingsley and J.R. Guerci, "Adaptive Amplifier Module Technique to Support Cognitive RF Architectures," Proceedings of the 2014 IEEE Radar Conference, Cincinnati, Ohio, May 2014, pp. 1329-1332.

[6] J.-S. Fu and A. Mortazawi, "Improving Power Amplifier Efficiency and Linearity Using a Dynamically Controlled Tunable Matching Network," *IEEE Transactions on Microwave Theory and Techniques*, Vol. 56, No. 12, December 2008, pp. 3239-3244.

[7] X. Liu, L.P.B. Katehi, W.J. Chappell, and D. Peroulis, "High-Q Tunable Microwave Cavity Resonators and Filters Using SOI-Based RF MEMS Tuners," *Journal of Microelectromechanical Systems*, Vol. 19, No. 4, August 2010, pp. 774-784.

[8] M. Abu Khater, Y.C. Wu, and D. Peroulis, "Tunable Cavity-Based Diplexer With Spectrum-Aware Automatic Tuning," *IEEE Transactions on Microwave Theory and Techniques*, Vol. 65, No. 3, pp. 934-944, March 2017.

[9] A. Semnani, M. Abu Khater, Y.-C. Wu, and D. Peroulis, "An Electronically-Tunable High-Power Impedance Tuner with Integrated Closed-Loop Control," *IEEE Microwave and Wireless Components Letters*, Vol. 27, No. 8, August 2017, pp. 754-756.

[10] A. Semani, D. Peroulis, and S. Macheret, "Plasma-Enabled Tuning of a Resonant RF Circuit," *IEEE Transactions on Plasma Science*, Vol. 44, No. 8, August 2016, pp. 1396-1404.

[11] C. Baylis, M. Fellows, L. Cohen, and R.J. Marks II, "Solving the Spectrum Crisis: Intelligent, Reconfigurable Microwave Transmitter Amplifiers for Cognitive Radar," *IEEE Microwave Magazine*, Vol. 15, No. 5, July 2014, pp. 94-107.

[12] M. Fellows, C. Baylis, J. Martin, L. Cohen, and R.J. Marks II, "Direct Algorithm for the Pareto Load-Pull Optimization of Power-Added Efficiency and Adjacent-Channel Power Ratio," *IET Radar, Sonar & Navigation*, Vol. 8, No. 9, December 2014, pp. 1280-1287.

[13] L. Hays, C. Kappelmann, S. Rezayat, A. Semnani, M. Abu Khater, D. Macias, A. Egbert, C. Baylis, D. Peroulis, E. Viveiros, and J. Penn, "Fast Circuit Optimization Using a Tunable Resonant Cavity Matching Circuit for Next-Generation Adaptive Radar Transmitter Applications," submitted to *IEEE Transactions on Aerospace and Electronic Systems*, October 2017.

[14] J. Barkate, M. Flachsbart, Z. Hays, M. Fellows, J. Barlow, C. Baylis, L. Cohen, and R.J. Marks II, "Fast, Simultaneous Optimization of Power Amplifier Input Power and Load Impedance for Power-Added Efficiency and Adjacent-Channel Power Ratio Using the Power Smith Tube," *IEEE Transactions on Aerospace and Electronic Systems*, Vol. 52, No. 2, April 2016, pp. 928-937.

[15] M. Fellows, L. Lamers, C. Baylis, L. Cohen, and R.J. Marks II, "Smith Tube Optimization of Drain Voltage and Load Reflection Coefficient to Maximize Power-Added Efficiency under ACPR Constraints," accepted August 2017 for publication in *IEEE Transactions on Aerospace and Electronic Systems*.

[16] Z. Hays, C. Kappelmann, L. Lamers, C. Baylis, M. Abu Khater, A. Semnani, D. Peroulis, E. Viveiros, and J. Penn, "Fast Impedance Matching Using Interval Halving of Resonator Position Numbers for a High-Power Evanescent-Mode Cavity Tuner," 2018 IEEE Radio and Wireless Symposium, Anaheim, California, January 2018.

[17] L. Hays, C. Kappelmann, S. Rezayat, A. Semnani, M. Abu Khater, D. Macias, A. Egbert, Z. Hays, C. Baylis, D. Peroulis, E. Viveiros, and J. Penn, "Fast Circuit Optimization Using a Tunable Resonant Cavity Matching Circuit for Next-Generation Adaptive Radar Transmitter Applications," submitted to *IEEE Transactions on Aerospace and Electronic Systems*, October 2017.